Acta Crystallographica Section B
Structural Science
ISSN 0108-7681

Basic forms of supramolecular self-assembly organized by parallel and antiparallel hydrogen bonds in the racemic crystal structures of six disubstituted and trisubstituted cyclopentane derivatives

Alajos Kálmán,[a]* Gyula Argay,[a] László Fábián,[a] Gábor Bernáth[b,c] and Ferenc Fülöp[c]

[a]Institute of Chemistry, Chemical Research Center, Hungarian Academy of Sciences, PO Box 17, Budapest 114, H-1525, Hungary, [b]Research Group for Heterocyclic Chemistry, Hungarian Academy of Sciences and University of Szeged, PO Box 121, Szeged H-6701, Hungary, and [c]Institute of Pharmaceutical Chemistry, University of Szeged, PO Box 121, Szeged H-6701, Hungary

Correspondence e-mail: akalman@chemres.hu

Received 30 November 2000
Accepted 6 April 2001

A selection of stereoisomeric 2-hydroxy-1-cyclopentanecarboxamides, a 4-*tert*-butyl derivative and three *tert*-butyl derivatives of the respective carboxylic acid were subjected to X-ray crystallography. The optically active molecules (I)–(VI) form racemic crystals. Each racemic structure is basically determined by two intermolecular hydrogen bonds of O—H···O=C—*X*H and O=C—*X*—H···OH types (*X* = O, NH). The partially similar patterns of close packing observed reflect five basic forms of supramolecular self-assembly. In the racemic crystals of chiral molecules, there are homo- and heterochiral chains of molecules formed by the principal (O—H···O=C) hydrogen bonds. These chains assemble either in a parallel or antiparallel mode. The parallel homochiral chains (hop) observed in structure (II), (1*R**,2*R**)-2-hydroxy-1-cyclopentanecarboxamide, demand the polar space group $Pca2_1$, while the parallel heterochiral chains (hep) are organized in antiparallel layers with space group $P2_1/n$ in structure (VI), (1*R**,2*S**,5*R**-5-*tert*-butyl-2-hydroxy-1-cyclopentanecarboxylic acid). Heterochiral chains in an antiparallel array (hea) are found in (I), (1*R**,2*S**)-2-hydroxy-1-cyclopentanecarboxamide, and (V) [(1*R**,2*S**4*S**)-4-*tert*-butyl-2-hydroxy-1-cyclopentanecarboxylic acid, space group $P2_1/c$]. Structures (IV), (1*R**,2*S**,4*R**)-4-*tert*-butyl-2-hydroxy-1-cyclopentanecarboxylic acid, and (III), (1*R**,2*R**,4*S**)-4-*tert*-butyl-2-hydroxy-1-cyclopentanecarboxamide, reveal that homochiral chains in an antiparallel array (hoa; cross-linked by heterochiral dimers held together by the second hydrogen bonds) can be formed by either translation (space group $P\bar{1}$) or a screw axis (space group $P2_1/c$). These alternatives are denoted hoa1 and hoa2. Similarly, within each pattern (hea, hep and hop) two slightly different alternatives can be expected. The partial similarities in the identified five patterns of hydrogen bonding are described by graph-set notations. Structures (I), (IV) and (V) can be characterized by a common supramolecular synthon, while the highest degree of similarity is shown by the isostructurality of (I) and (V).

1. Introduction

In the course of a systematic study of *tert*-butylcyclopentane-fused 1,3-oxazines, thiazines and pyrimidin-4(3*H*)-ones (Bernáth *et al.*, 1994; Szakonyi *et al.*, 1996), six intermediate cyclopentane derivatives (Fig. 1) were subjected to single-crystal X-ray diffraction analysis. The endocyclic bond lengths and angles corresponded with the standard values given in the Cambridge Structural Database (Allen & Kennard, 1993). The presence of the *tert*-butyl moiety in (III)–(VI) slightly increases the lengths of the bonds involving the substituent-

bearing C atom (by *ca* 0.02 Å), while the corresponding endocyclic bond angle is decreased (by *ca* 2°). Similarly, the torsion angles exhibit differences, *e.g.* between the 1,2-*cis* and *trans* stereoisomers.

The range of structural variety observed at a molecular level is conceptually extended if these crystal structures are regarded as supermolecular assemblies governed by intermolecular interactions. The simplicity of structures (I)–(VI) offers an opportunity to study intermolecular hydrogen-bond interactions generated by two vicinal (*cis* or *trans*) functions (OH *versus* $CONH_2$ or OH *versus* COOH) located on a cyclopentane ring with limited flexibility. Each 2-hydroxy-1-cyclopentanecarboxylic acid forms only two intermolecular hydrogen bonds, while each 2-hydroxy-1-cyclopentanecarboxamide forms three. In each of the six structures, there is one common O—H···O hydrogen bond between the 2-OH group and the 1-CO O atom of a symmetry-equivalent molecule. In response to this, both the COOH (IV)–(VI) and $CONH_2$ moieties (I)–(III) donate a second X—H···O hydrogen bond to the 2-OH group of another molecule. In (I)–(III) the $CONH_2$ moiety is bifunctional: one of its N—H arms replaces the OH function in the second O—H···O hydrogen bond of (IV)–(VI), whereas the remaining N—H arm forms a third intermolecular hydrogen bond with the carbonyl O atom from a neighboring molecule. These hydrogen bonds are independent of the stereoisomerism and/or substitutional isomerism exhibited by these compounds. Only their symmetry is dependent on the stereostructure (*i.e.* the *cis*/*trans* isomerism) of the molecules and the position of the bulky *tert*-butyl moiety. Every crystal is *racemic* and, therefore, each diastereomer has the same amount (1:1) of its enantiomer in the unit cell. Each asymmetric unit contains only one molecule and no intramolecular hydrogen bonds are formed. The interdependence of the O—H···O(=C) and X—H···OH hydrogen bonds per structure prompted us to analyse the forms of molecular self-complementarity by the use of graph-set notations (Etter, 1990; Bernstein *et al.*, 1995) and, whenever appropriate, by the assignment of common or similar supramolecular synthons (Desiraju, 1995, 1997). Overall, the six structures reflect five basic forms of supramolecular self-assembly organized by parallel or antiparallel arrangement of hydrogen-bonded homo- and heterochiral chains, and revealed an unusual isostructurality (Kálmán *et al.*, 1993) between structures (I) and (V).

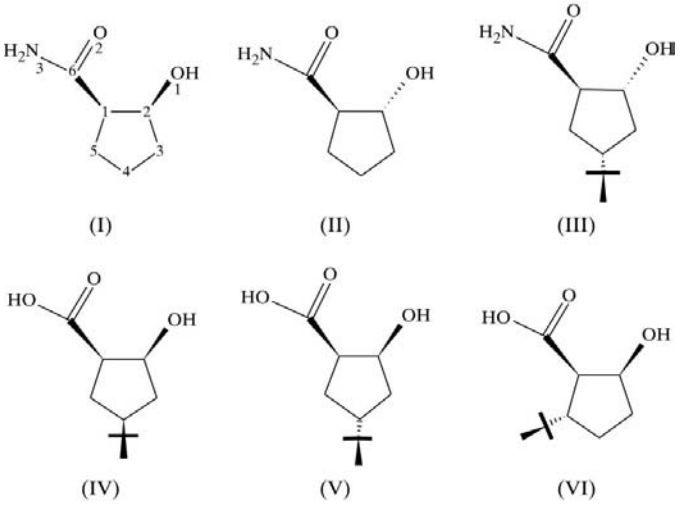

Figure 1
Chemical structures of the six related molecules showing their stereoisomerism. The common and relevant atomic numbering is given on (I).

2. Experimental

2.1. Synthesis

The synthesis, characterization and several chemical transformations of (I)–(VI) have been reported earlier (Bernáth & Svoboda, 1972; Bernáth *et al.*, 1972; Fülöp *et al.*, 1994; Riddell *et al.*, 1995).

2.2. Data collection, structure solution and refinement

Details of the cell data, data collection and refinement are provided in Table 1.[1] Each data set was collected on a CAD-4 diffractometer equipped with a graphite monochromator. Lattice parameters were refined by a least-squares fit for 25 reflections. Standard reflections (three for each data collection) indicated 2% decay only in the crystals of (I). All reflections were corrected for Lorenz and polarization effects. The space groups were determined from unit-cell symmetry, systematic absences and refinement (II). The crystallographic phase problem was solved by direct methods, using the programs *SHELXS*86 and *SHELXS*97 (Sheldrick, 1985, 1997*a*). The atomic positions for each structure were refined with anisotropic displacement parameters in the F^2 mode, using the program *SHELXL*97 (Sheldrick, 1997*b*). The positions of the H atoms bound either to O or to N atoms were located in difference-Fourier maps, while the others were generated from assumed geometries and were refined isotropically in the riding mode. The absolute structure of (II) in the polar space group $Pca2_1$ was determined by refining the Flack parameter (Flack, 1983).

As part of the cooperation between our laboratories, structures of the intermediates (III)–(VI) had been solved in 1991 to check their expected stereoisomerism. With reflections/parameters > 10 the refinements were then regarded as satisfactory. In the meantime, in an independent work reported by Riddell *et al.* (1995) structure (VI) was accidentally redetermined (R = 0.068, wR = 0.064 for 2070 unique reflections). Recently, the configurational polymorphism (Dunitz & Bernstein, 1995) of the diastereomeric molecules (I) and (II) prompted us to extend the hydrogen-bond studies on structures (III)–(VI). Despite the observed high R_1 values [in particular for (III)], the relevant hydrogen positions could be located unambiguously in difference maps. Since the original structure analysis of (VI) had resulted in R = 0.047, wR = 0.124 for 2204 unique reflections, the present paper is based on the earlier structure determination.

[1] Supplementary data for this paper are available from the IUCr electronic archives (Reference: DE0011). Services for accessing these data are described at the back of the journal.

3. Results and discussion

3.1. Survey of the structures at a molecular level

The molecular structures of the six 2-hydroxycyclopentanes are depicted in Fig. 2. The six compounds can be classified in terms of *cis–trans* isomerism, the absence or presence of the bulky *tert*-butyl moiety and OH → NH_2 replacement in the CO*X* group. The *tert*-butyl function (III)–(VI), the $CONH_2$ group (I)–(III) and the COOH group (IV)–(VI) are always *pseudo*-equatorial. The *cis* or *trans* isomerism along the C1—C2 bond is shown by the *pseudo*-axial (I), (IV)–(VI) or equatorial (II) and (III) orientation of the 2-OH function. From this, it follows that the C6—C1—C2—O1 torsion angle (Table 2) is substantially larger (*ca* 73°) in the 1,2-*trans* isomers (II) and (III) than in the *cis* isomers (43–52°).

Molecules (I) and (II), containing no *tert*-butyl substituent, are diastereomers, and according to Dunitz & Bernstein (1995) their crystals can be regarded as configurational polymorphs. In (I) puckering of the flexible cyclopentane ring, *via* pseudorotation (Altona *et al.*, 1968), results in an almost perfect $C_s(2)$ envelope shape (the corresponding puckering parameters introduced by Cremer & Pople, 1975, are listed in Table 2). In (II) the cyclopentane ring with its two 1,2-*trans* functions assumes a conformation that is intermediate between the $C_s(2)$ and $C_2(4)$ forms, whereas in (III) the ring puckering gives a nearly perfect $C_2(4)$ half-chair. Molecules (IV) and (V) are also diastereomers. The cyclopentane ring in (IV) is a $C_s(1)$ envelope form, while the planar COOH group is eclipsed with the C1—C5 bond (Table 2). In (V) the COOH group remains eclipsed with the C1—C5 bond, but the cyclopentane ring, similarly as in (I), changes from a $C_s(1)$ into a $C_s(2)$ envelope with the 2-OH group on the flap. Transfer of the *tert*-butyl moiety from C4 to C5 results in (VI). The juxtaposition of the *tert*-butyl and the planar COOH groups induces a rotation of *ca* 15° of the COOH group about the C1—C6 bond, which is accompanied by a pseudorotation from the nearly perfect $C_s(1)$ envelope found in (V) to a transitional state between a $C_s(2)$ envelope and a $C_2(5)$ half-chair.

3.2. Hydrogen-bond networks

3.2.1. Packing motifs and patterns. A survey of the intermolecular relationships exhibited by the molecules confirmed that, besides some conformational differences, similarities can be observed in the forms of supramolecular self-organization mediated by two, chemically different hydrogen bonds (Table 3). The common O1—H···O2 hydrogen bonds are formed along glide planes (*g*) in three structures (I), (V) and (VI), with translation (*t*) in (IV), whereas they form helices (2_1) in both *trans* isomers (II) and (III). Glide planes generate heterochiral meanders (*M*), while translation and screw axes form homochiral tapes (*T*) and helices (*H*). The second *X*3—H···O1 hydrogen bonds, in addition to a screw axis [for (I) and (V)] and glide plane [for (II) and (VI)], form heterochiral *rings* (*R*) around inversion centers in (III) and (IV). This means that the O1—H···O2 hydrogen bonds do not form an *R* motif, while the *X*3—H···O1 hydrogen bonds do not form a *T* motif. Overall, the six structures demonstrate five independent racemic patterns of close packing in which the three chain motifs of the common O1—H···O2 hydrogen bond are parallel or antiparallel. Since both homochiral chains (*T* and *H*) may assume an antiparallel array [(IV) and (III)], the pattern hoa covers two alternatives, hoa1 and hoa2. Similarly, both *H* and *T* chains may also be parallel. These patterns are termed hop1 and hop2. In (II) the parallel helices with opposite chirality (hop1) generate parallel glide planes in a polar space group $Pca2_1$. In hop2 motifs *H* are replaced by motifs *T*. Structures (I) and (V) reflect the pattern hea1, in which

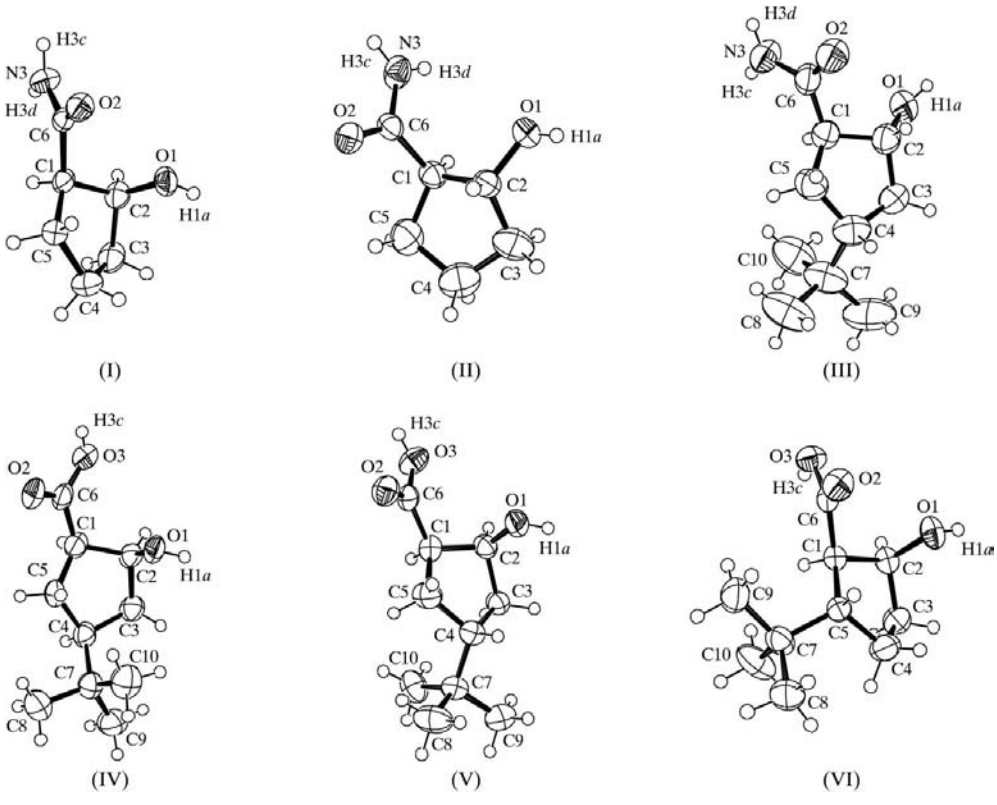

Figure 2
Molecular structures of (I)–(VI), showing their common atomic numbering. Only the H atoms with distinguished function are numbered. The enantiomers presented are in agreement with the chemical formulae depicted in Fig. 1.

Table 1
Experimental details.

	(I)	(II)	(III)
Crystal data			
Chemical formula	$C_6H_{11}NO_2$	$C_6H_{11}NO_2$	$C_{10}H_{19}NO_2$
Chemical formula weight	129.16	129.16	185.26
Cell setting, space group	Monoclinic, $P2_1/c$	Orthorhombic, $Pca2_1$	Monoclinic, $P2_1/c$
a, b, c (Å)	11.693 (2), 7.225 (1), 7.902 (2)	9.879 (2), 8.410 (2), 8.250 (2)	13.246 (5), 6.988 (2), 13.299 (6)
β (°)	103.70 (3)	90	113.78 (8)
V (Å^3)	648.6 (2)	685.4 (3)	1126.5 (7)
Z	4	4	4
D_x (Mg m^{-3})	1.323	1.252	1.092
Radiation type	Cu $K\alpha$	Cu $K\alpha$	Mo $K\alpha$
No. of reflections for cell parameters	25	25	25
θ range (°)	26.08–29.89	17.48–24.14	10.0–12.61
μ (mm^{-1})	0.819	0.775	0.075
Temperature (K)	293 (2)	293 (2)	293 (2)
Crystal form, color	Block, colorless	Block, colorless	Block, colorless
Crystal size (mm)	0.30 × 0.15 × 0.08	0.15 × 0.12 × 0.05	0.55 × 0.30 × 0.15
Data collection			
Diffractometer	Enraf–Nonius CAD-4	Enraf–Nonius CAD-4	Enraf–Nonius CAD-4
Data collection method	ω–2θ scans	ω–2θ scans	ω–2θ scans
Absorption correction	Psi scan	Psi scan	Psi scan
T_{min}	0.7913	0.944	0.9599
T_{max}	0.9374	1.000	0.9888
No. of measured, independent and observed parameters	1431, 1274, 1149	1569, 1375, 1145	2449, 2350, 844
Criterion for observed reflections	$I > 2\sigma(I)$	$I > 2\sigma(I)$	$I > 2\sigma(I)$
R_{int}	0.0170	0.0089	0.0180
θ_{max} (°)	74.91	74.78	26.97
Range of h, k, l	$-14 \rightarrow h \rightarrow 14$ $-9 \rightarrow k \rightarrow 0$ $0 \rightarrow l \rightarrow 9$	$-12 \rightarrow h \rightarrow 12$ $-10 \rightarrow k \rightarrow 10$ $-9 \rightarrow l \rightarrow 10$	$-16 \rightarrow h \rightarrow 15$ $0 \rightarrow k \rightarrow 8$ $0 \rightarrow l \rightarrow 16$
No. and frequency of standard reflections	3 every 60 min	3 every 60 min	3 every 60 min
Intensity decay (%)	2	0	0
Refinement			
Refinement on	F^2	F^2	F^2
$R[F^2>2\sigma(F^2)]$, $wR(F^2)$, S	0.0406, 0.1272, 1.138	0.034, 0.1133, 0.86	0.0502, 0.1657, 0.948
No. of reflections and parameters used in refinement	1274, 84	1375, 83	2350, 123
H-atom treatment	Mixed	Mixed	Mixed
Weighting scheme	$w = 1/[\sigma^2(F_o^2) + (0.1000P)^2 + 0.0000P]$, where $P = (F_o^2 + 2F_c^2)/3$	$w = 1/[\sigma^2(F_o^2) + (0.1000P)^2 + 0.0000P]$, where $P = (F_o^2 + 2F_c^2)/3$	$w = 1/[\sigma^2(F_o^2) + (0.0020P)^2 + 6.5000P]$, where $P = (F_o^2 + 2F_c^2)/3$
$(\Delta/\sigma)_{max}$	0.000	0.000	0.000
$\Delta\rho_{max}$, $\Delta\rho_{min}$ (e Å^{-3})	0.308, −0.172	0.127, −0.134	0.265, −0.251
Extinction method	*SHELXL*97 (Sheldrick, 1997*b*)	None	*SHELXL*97 (Sheldrick, 1997*b*)
Extinction coefficient	0.026 (5)	–	0.062 (6)

	(IV)	(V)	(VI)
Crystal data			
Chemical formula	$C_{10}H_{18}O_3$	$C_{10}H_{18}O_3$	$C_{10}H_{18}O_3$
Chemical formula weight	186.24	186.24	186.24
Cell setting, space group	Triclinic, $P\overline{1}$	Monoclinic, $P2_1/c$	Monoclinic, $P2_1/n$
a, b, c (Å)	5.931 (1), 6.200 (1), 15.951 (3)	16.862 (2), 6.104 (1), 10.519 (3)	6.170 (2), 21.749 (2), 7.892 (1)
α, β, γ (°)	84.30 (4), 89.97 (4), 62.28 (4)	90, 107.03 (4), 90	90, 105.57 (4), 90
V (Å^3)	515.97 (15)	1035.2 (4)	1020.2 (4)
Z	2	4	4
D_x (Mg m^{-3})	1.199	1.195	1.213
Radiation type	Mo $K\alpha$	Cu $K\alpha$	Mo $K\alpha$
No. of reflections for cell parameters	25	25	25
θ range (°)	11.0–13.2	24.50–28.30	10.28–13.14
μ (mm^{-1})	0.087	0.704	0.088
Temperature (K)	293 (2)	293 (2)	293 (2)
Crystal form, color	Block, colorless	Block, colorless	Block, colorless
Crystal size (mm)	0.40 × 0.20 × 0.09	0.35 × 0.20 × 0.12	0.40 × 0.25 × 0.12

Table 1 (continued)

	(IV)	(V)	(VI)
Data collection			
Diffractometer	Enraf–Nonius CAD-4	Enraf–Nonius CAD-4	Enraf–Nonius CAD-4
Data collection method	ω–2θ scans	ω–2θ scans	ω–2θ scans
Absorption correction	Psi scan	Psi scan	Psi scan
T_{min}	0.9661	0.7913	0.9658
T_{max}	0.9922	0.9374	0.9896
No. of measured, independent and observed parameters	3107, 2998, 1971	2137, 2084, 1598	2276, 2204, 1239
Criterion for observed reflections	$I > 2\sigma(I)$	$I > 2\sigma(I)$	$I > 2\sigma(I)$
R_{int}	0.0193	0.0215	0.0160
θ_{max} (°)	29.95	74.99	26.96
Range of h, k, l	$0 \rightarrow h \rightarrow 8$ $-7 \rightarrow k \rightarrow 8$ $-22 \rightarrow l \rightarrow 22$	$0 \rightarrow h \rightarrow 21$ $0 \rightarrow k \rightarrow 7$ $-13 \rightarrow l \rightarrow 12$	$0 \rightarrow h \rightarrow 7$ $0 \rightarrow k \rightarrow 27$ $-10 \rightarrow l \rightarrow 9$
No. and frequency of standard reflections	3 every 60 min	3 every 60 min	3 every 60 min
Refinement			
Refinement on	F^2	F^2	F^2
$R[F^2>2\sigma(F^2)]$, $wR(F^2)$, S	0.0477, 0.1776, 1.147	0.0541, 0.1688, 0.951	0.0474, 0.1875, 0.932
No. of reflections and parameters used in refinement	2998, 124	2084, 125	2204, 124
H-atom treatment	Mixed	Mixed	Mixed
Weighting scheme	$w = 1/[\sigma^2(F_o^2) + (0.0626P)^2 + 0.1708P]$, where $P = (F_o^2 + 2F_c^2)/3$	$w = 1/[\sigma^2(F_o^2) + (0.1017P)^2 + 0.4219P]$, where $P = (F_o^2 + 2F_c^2)/3$	$w = 1/[\sigma^2(F_o^2) + (0.0300P)^2 + 0.8000P]$, where $P = (F_o^2 + 2F_c^2)/3$
$(\Delta/\sigma)_{max}$	0.000	0.000	0.002
$\Delta\rho_{max}$, $\Delta\rho_{min}$ (e Å^{-3})	0.3, −0.268	0.249, −0.241	0.257, −0.24
Extinction method	*SHELXL*97 (Sheldrick, 1997*b*)	*SHELXL*97 (Sheldrick, 1997*b*)	*SHELXL*97 (Sheldrick, 1997*b*)
Extinction coefficient	0.029 (11)	0.0019 (9)	0.019 (4)

Computer programs used: *CAD*-4 *EXPRESS* (Enraf–Nonius, 1992), *XCAD*4 (Harms, 1996), *SHELXS*86 (Sheldrick, 1985), *SHELXS*97 (Sheldrick, 1997*a*), *SHELXL*97 (Sheldrick, 1997*b*), *PLUTO* in CSD (Allen & Kennard, 1993), *PLATON* (Spek, 1998).

the *M* motifs are cross-linked by *H* motifs. The latter motifs can readily be replaced by *R* motifs and this pattern is denoted hea2. Finally, in (VI) the *M* motifs (hep1) are cross-linked by other *M* motifs; both are formed by the same glide plane *n*. *Mutatis mutandis*, two parallel glide planes (*a* and *c* or *n* and *c*), may also form an independent pattern denoted as hep2. The six structures are discussed below in terms of these basic packing modes.

3.2.2. Carboxylic acids (IV), (V) and (VI). The structures (IV), (V) and (VI) differ only in the position of the bulky *tert*-butyl moiety, which results in three packing modes: hoa1, hea1 and hep1. The simplest form of hydrogen bonding is organized by translation and inversion centers in a triclinic unit cell with space group $P\bar{1}$. This may be attributed to the unique feature of molecule (IV), that all COOH, OH and *tert*-butyl groups are on the same face of the cyclopentane ring. In the triclinic unit cell (Table 1), the homochiral row of translation-related (IV) molecules (*T* motif) is accompanied by an antiparallel row of the enantiomers (Fig. 3). These rows are cross-linked by the second O3—H···O1 hydrogen bonds donated from the 1-COOH groups to the 2-OH moieties (pattern hoa1). Each cross-link is an $R_2^2(12)$ ring (Etter, 1990) and is formed around $\bar{1}$ at $0,\frac{1}{2},\frac{1}{2}$ and $1,\frac{1}{2},\frac{1}{2}$, respectively. Additionally, there is a second 12-membered ring around another inversion center at $\frac{1}{2},\frac{1}{2},\frac{1}{2}$. This $R_4^4(12)$ ring is a tetramer, which is formed between two COOH and two OH groups. In the monoclinic unit cell of (V) (Fig. 4), the *M* motif replaces the *T* motif; both are built up by the same O1—H···O2 hydrogen bonds. Since the homochiral chains become heterochiral, the center of inversion-related $R_2^2(12)$ rings of (IV) turn into infinite $C(6)$ (Etter, 1990) helices (*H*) around 2_1 ($\frac{1}{2}$, *y*, $\pm\frac{1}{4}$) *etc*. The result is a close packing in the

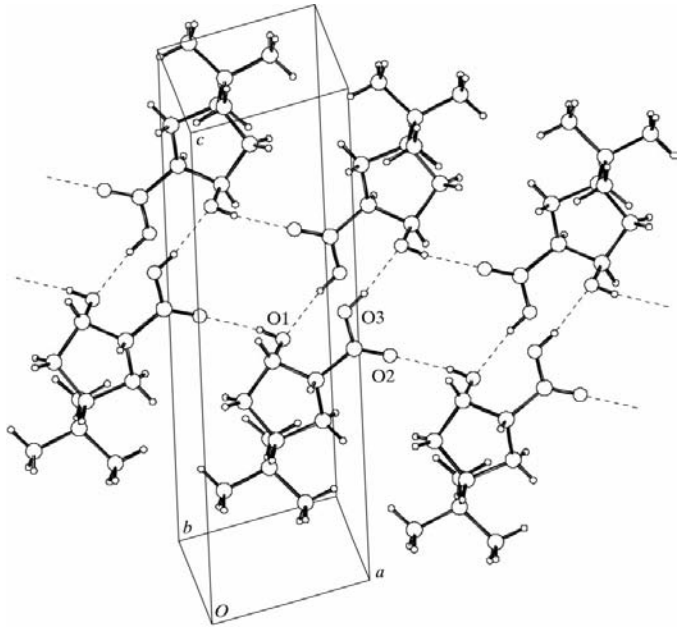

Figure 3
Perspective view of the crystal structure (IV), showing a translation-generated row of homochiral molecules opposed by a row of $\bar{1}$ (1, $\frac{1}{2}$, $\frac{1}{2}$) center of inversion-related enantiomers. Both $R_2^2(12)$ and $R_4^4(12)$ [synthon (1a)] rings can be observed.

Table 2
Relevant torsion angles and puckering parameters (Cremer & Pople, 1975) of the cyclopentane rings in (I)–(VI).

	C6—C1—C2—O1	O2—C6—C1—C5	φ (°)	Q (Å)			Shape
(I)	48.7 (1)	−29.5 (1)	35.2 (2)	0.408 (2)	C_s(2)		Envelope
(II)	73.1 (2)	−36.9 (3)	25.0 (5)	0.387 (2)	C_s(2)	C_2(4)	Transitional form
(III)	72.7 (3)	−73.2 (3)	17.2 (5)	0.416 (4)		C_2(4)	Half-chair
(IV)	48.5 (2)	−5.6 (2)	1.3 (4)	0.403 (2)	C_s(1)		Envelope
(V)	−51.5 (2)	3.6 (2)	32.5 (5)	0.399 (2)	C_s(1)		Envelope
(VI)	43.4 (2)	17.2 (3)	46.6 (5)	0.388 (4)	C_s(2)	C_2(5)	Transitional form

space group $P2_1/c$, where the symmetry operators c and 2_1 separately govern the formation of the O1—H···O2 and O3—H···O1 hydrogen bonds. The crystals of the diastereomeric pair (IV) and (V) have the same packing coefficient (Gavezzotti, 1983) of 0.68 and there is a visible packing similarity between them. In both the triclinic and the monoclinic unit cells, identical $R_4^4(12)$ rings can be discerned around appropriately chosen inversion centers. This ring can be regarded as a tetrameric supramolecular synthon [termed (1a); Kálmán *et al.*, 2000], an enlarged form of the most common synthon (1) (Fig. 5) listed by Desiraju (1995).

This relationship between (V) and (IV) can be visualized by the use of graphical symbols (*e.g.* asymmetric black and white arrows) for the molecules. In Fig. 6(*a*), two antiparallel (in the direction of the chain) *T* motifs of enantiomers are connected simultaneously by $R_2^2(12)$ dimers and $R_4^4(12)$ tetramers. When a change in chirality at C4 brings the *tert*-butyl group to the other side of the ring, a new molecular self-complementarity is established (Fig. 6*b*). The lower and upper chains (*M*) are cross-linked by *H* motifs. Between the C(6) helices there are the $R_4^4(12)$ tetramers. If the upper chain is shifted by *ca* $\frac{1}{2}$ of its period in either direction, an alternative pattern can be established: the tetramers are replaced by the $R_2^2(12)$ dimers. However, the row of $R_2^2(12)$ dimers and $R_4^4(12)$ tetramers found in (IV) is restored if the screw axes are replaced by twofold axes (Fig. 6*c*), which in general are less favorable in close packing than the helical arrays (Zorky, 1993; Brock & Dunitz, 1994). The new space group is *C*2/*c*. This packing mode (hea2) is not present among the six structures, but is expected to be found among the isomers and analogues of molecules (IV) and (V).

Transfer of the *tert*-butyl group from C4 to C5 converts (V) into (VI). The juxtaposition of the bulky *tert*-butyl and the COOH groups results in a basically different packing array

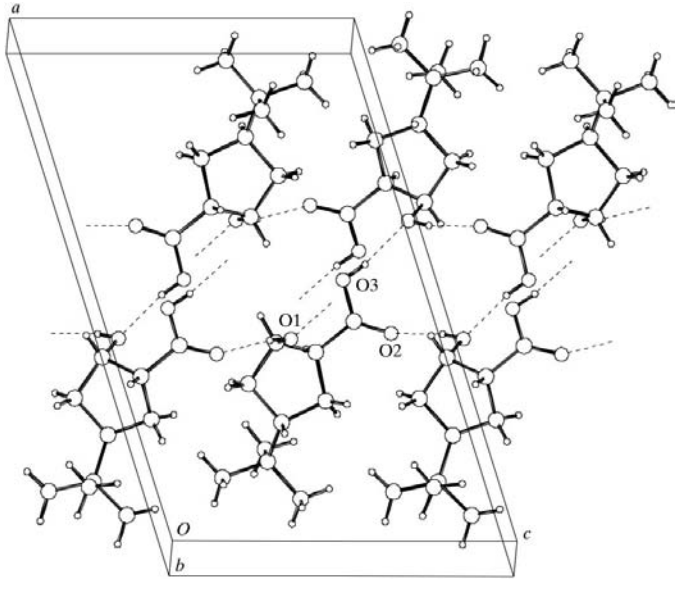

Figure 4
Perspective view of the crystal structure of (V), showing a glide plane-related row of heterochiral molecules. The central pair is homochiral and related by a 2_1 screw axis at ($\frac{1}{4}$, *y*, $\frac{1}{2}$), leading to an infinite helix of *C*(6) type around the *b* axis. The $R_4^4(12)$ ring [synthon (1a)] can also be recognized.

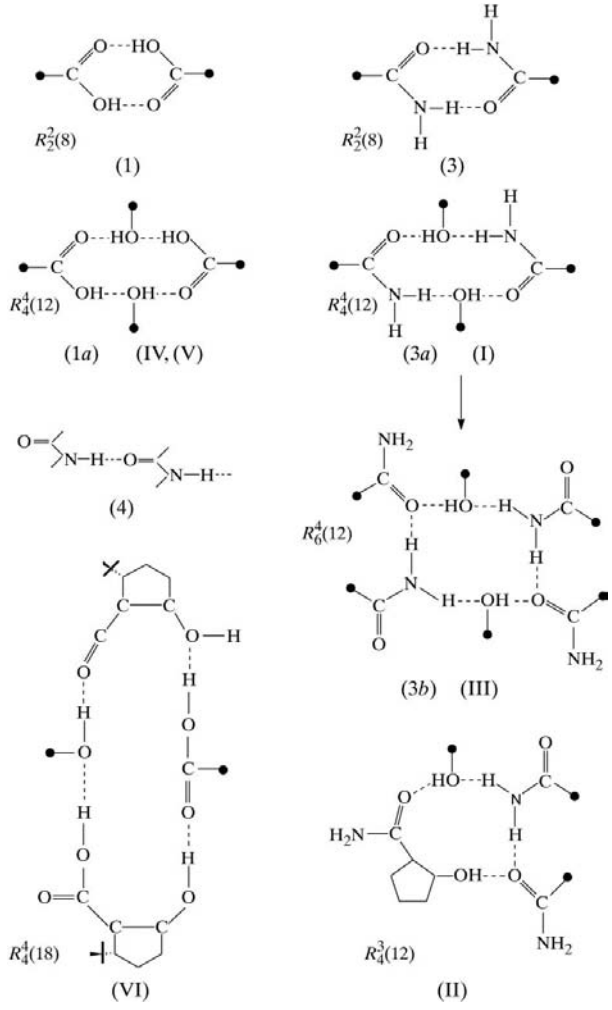

Figure 5
Supramolecular synthons (1), (3) and (4), as listed by Desiraju (1995), and their enlarged forms (1a) and (3a) found in (IV), (V) and (I), respectively, and analogous rings revealed in (II), (III) and (VI).

(VI), with a packing coefficient of 0.69, similar to those of (IV) and (V). The molecules are arranged in thin zigzag layers stretching diagonally in the monoclinic unit cell parallel to the *b* axis (Fig. 7). The *M* motifs built up by O1—H···O2 hydrogen-bonded molecules (dashed lines in Fig. 8) are arranged in a parallel mode. These chains are cross-connected by the O3—H···O1 hydrogen bonds (dotted lines). Each white arrow assumes a central position between the translation-equivalent black arrows on the four corners of an idealized unit cell. From the individual *C*(6) chains, three glide-plane-related molecules form a $C_2^2(6)$ chain, while four molecules form a large $R_4^4(18)$ ring (Fig. 5). The opposite directions of the four hydrogen bonds generate an antidromic ring, which, according to Jeffrey & Saenger (1991), has a significant total dipole moment. Since dipoles must cancel out over the whole crystal, antiparallel stacking of the layers is compulsory. The antiparallel stacking of layers depicted in Fig. 8 gives rise to an elongated *b* axis *via* inversion centers with space group $P2_1/n$, from which it follows that in (VI) there are no hydrogen-bonded connections between the hep1 layers. They are linked only by weak van der Waals interactions. Otherwise, the parallel stacking of the layers would correspond with a rare (0.4%) polar space group, *Pc*.

So far, we have seen how the different positions of the *tert*-butyl group lead to the formation of three types of close packing. One of them (IV) is triclinic, while two [(V) and (VI)] are monoclinic. The question of why the O1—H···O2 hydrogen bonds in (IV) are formed with translation rather than with glides planes was answered by modeling the close packing of the all-*cis* (IV) molecules in structure (V). This arrangement is hindered by very short H···H contacts of ∼1.15 Å.

3.2.3. Carboxamides (III), (II) and (I). Replacement of the *cis*-COOH group by a *trans*-$CONH_2$ moiety introduces two novel patterns of hydrogen bonding:

(i) In both structures (III) and (II) the C6—C1—C2—O1 torsion angle is opened by 25° up to *ca* 73.° As a result, the principal hydrogen bonds link molecules along screw axes. These helices (*H*), with either (1*R*,2*R*) or (1*S*,2*S*) chirality, can be parallel or antiparallel. The antiparallel helices in (III) are related by $\bar{1}$ symmetry, resulting once again in the space group $P2_1/c$. The parallel helices are separated by glide plane(s) in

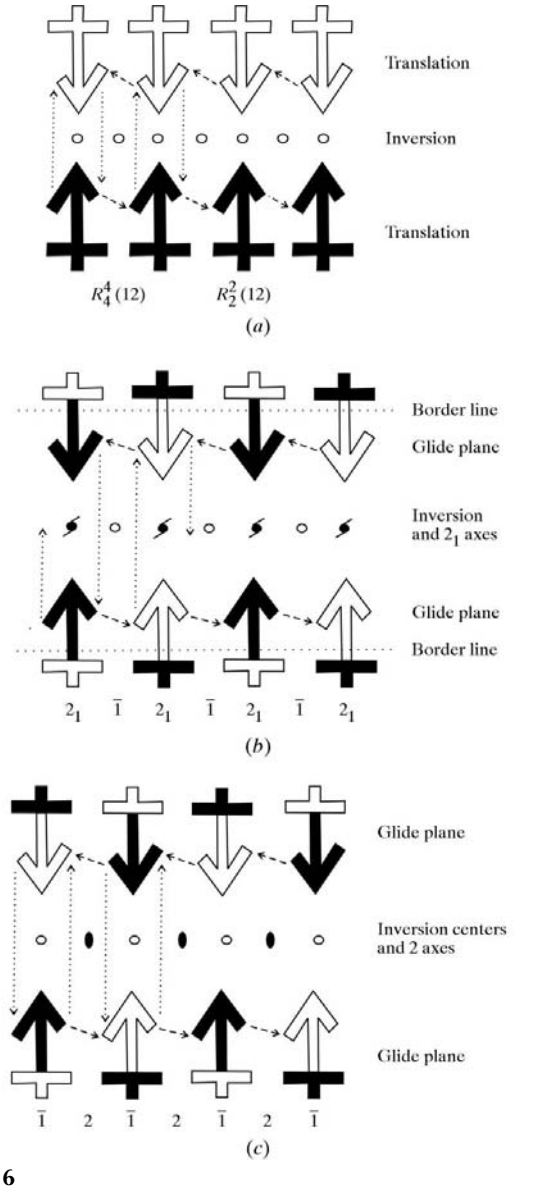

Figure 6
Schematic diagram of patterns hoa1 and hea1 found in (IV) and (V). The long and short arrowheads represent the 1-COOH and 2-OH functions, while color distinguishes the enantiomers. Mixed color refers to stereoisomerism around C4. (*a*) All-*cis* diastereomer (IV). The separate homochiral tapes (*T*) of the enantiomers are cross-linked across centers of inversion (hoa1). They alternately form $R_2^2(12)$ dimers and $R_4^4(12)$ tetramers. (*b*) Diastereomer (V). The *tert*-butyl groups on the opposite side are shown by a black cross *versus* a white arrow and *vice versa*. The heterochiral meanders (*M*) are cross-linked *via* homomolecular pairs around 2_1 screw axes (hea1), while the inversion centers generate the $R_4^4(12)$ tetramers as in (IV). (*c*) A shift of the upper row by $\frac{1}{2}$ of the translation leads to a novel pattern (hea2) if the screw axes are replaced simultaneously by twofold rotations. Both $R_4^4(12)$ tetramers and $R_2^2(12)$ dimers are preserved.

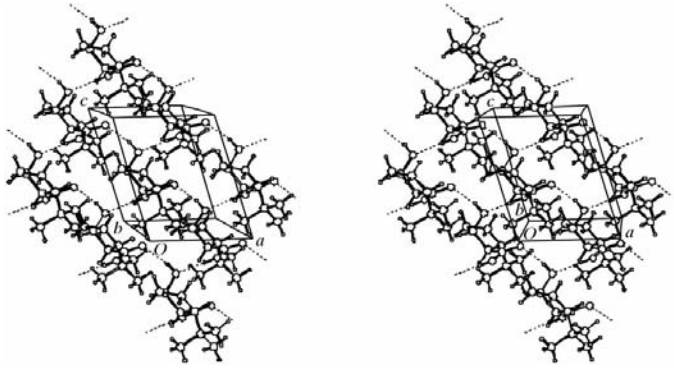

Figure 7
Stereoview of the crystal structure (VI), showing compact diagonal zigzag stripes of the O1—H···O2 hydrogen-bonded molecules interconnected *via* the O3—H···O1 hydrogen bonds. Both *M* motifs (perpendicular to each other) are formed by the same $n(x, \frac{1}{4}, z)$ glide plane, which generates two molecules from the reference molecule $M_{(x,y,z)}$ with coordinates $x - \frac{1}{2}$, $-y + \frac{1}{2}$, $z \pm \frac{1}{2}$. Their unit ($\Delta z = 1$) separation provides the spatial condition to form both O—H···O hydrogen bonds along the same glide plane.

Table 3
Hydrogen bonds and their descriptors.

The symmetry codes given in rows 2, 7 and 12 refer to the acceptor atoms of hydrogen bonds.

	(I)	(II)	(III)	(IV)	(V)	(VI)
O1—H1(*xyz*)···O2	$x, -\frac{1}{2}-y, -\frac{1}{2}+z$	$-x, -y, \frac{1}{2}+z$	$2-x, -\frac{1}{2}+y, \frac{1}{2}-z$	$-1+x, 1+y, z$	$x, \frac{1}{2}-y, -\frac{1}{2}+z$	$-\frac{1}{2}+x, \frac{1}{2}-y, \frac{1}{2}+z$
D···*A* (Å)	2.859 (1)	2.751 (2)	2.719 (3)	2.786 (2)	2.855 (2)	2.738 (2)
H···*A* (Å)	2.07	1.93	1.90	1.97	2.04	1.94
D—H···*A* (°)	162.2	173.3	176.4	170.2	170.8	163.7
Symmetry operator	Glide plane	Screw axis	Screw axis	Translation	Glide plane	Glide plane
N3—H3*c*(*xyz*)···O1	$-x, \frac{1}{2}+y, \frac{1}{2}-z$	$\frac{1}{2}-x, y, -\frac{1}{2}+z$	$2-x, -y, 1-z$			
O3—H(*xyz*)···O1				$2-x, 1-y, 1-z$	$1-x, -\frac{1}{2}+y, \frac{3}{2}-z$	$-\frac{1}{2}+x, \frac{1}{2}-y, -\frac{1}{2}+z$
D···*A* (Å)	3.030 (1)	2.964 (2)	2.913 (3)	2.664 (2)	2.686 (2)	2.702 (2)
H···*A* (Å)	2.17	2.11	2.08	1.85	1.88	1.89
D—H···*A* (°)	172.7	169.7	162.1	169.5	166.3	171.2
Symmetry operator	Screw axis	Glide plane	Inversion center	Inversion center	Screw axis	Glide plane
N3—H3*d*(*xyz*)···O2	$x, \frac{1}{2}-y, -\frac{1}{2}+z$	$\frac{1}{2}-x, y, \frac{1}{2}+z$	$2-x, \frac{1}{2}+y, \frac{1}{2}-z$			
D···*A* (Å)	3.102 (1)	2.951 (2)	2.964 (3)			
H···*A* (Å)	2.28	2.10	2.14			
D—H···*A* (°)	160.3	169.3	160.5			
Symmetry operator	Glide plane	Glide plane	Screw axis			

(II) and together generate an orthorhombic space group $Pca2_1$ (No. 29), which is 50 times less frequent than $P2_1/c$. These crystal structures represent the packing modes hoa2 and hop1.

(ii) In both (II) and (III) the complementary second N3—H···O1 hydrogen bonds are maintained by the NH_2 groups, while their second arms form the third hydrogen bond with the CO groups of appropriately located neighboring molecules (*see below*).

The difference between the parallel and antiparallel arrays of the helices formed by the enantiomeric molecules (black and white) is demonstrated by graphical symbols. To give a better view of the molecules around the screw axes, the arrows (Figs. 6 and 8) are replaced by their projections. The sharp point of a triangle represents the 2-OH group, while the small circle and small triangle denote the O atom and the NH_2 group, respectively. In (III) (Fig. 9) antiparallel helices in pairs are cross-linked by dimers (*R* motifs) formed around $\bar{1}$ $(0,0,\frac{1}{2})$ and its translation-equivalent points along the *b* axis. The folded $R_2^2(12)$ dimers are joined by the N3—H3*c*···O1 hydrogen bonds (Fig. 5). The third hydrogen bond, N3—H3*d*···O2, is perfectly embedded in this network. Together

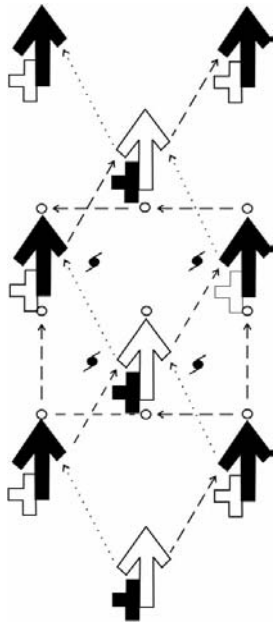

Figure 8
Pattern hep1: heterochiral chains (*M*) in a parallel array. One white arrow is connected to four black arrows *via* O1—H···O2 and O3—H···O1 hydrogen bonds. Two white and two black arrows complete the antidromic $R_4^4(18)$ ring. The position of the *tert*-butyl group (black cross) on the cyclopentane ring is symbolized by a modified (white) arrow.

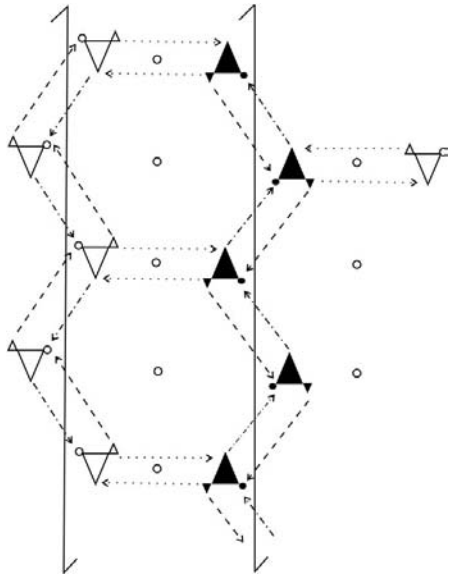

Figure 9
Pattern hoa2: antiparallel helices in (III) cross-linked around inversion centers into $R_2^2(12)$ dimers. Between two dimers separated by $\Delta y = 1$, a six-membered ring is formed by three molecules from each helix. Around each screw axis, a double helix is formed by O1—H···O2 and N3—H3···O2 hydrogen bonds. Together with the $R_2^2(12)$ dimers they form an inner $R_6^4(12)$ ring and an outer $R_6^6(32)$ ring. Ignoring the N3—H3···O2 contacts, an intermediate homodromic $R_6^6(24)$ ring can be recognized.

with the principal hydrogen bond, it forms double helices around the antiparallel screw axes. The graph-set notations are $C(6)$ and $C(4)$, respectively. Together, the three types of hydrogen bond form a corrugated two-dimensional chicken-wire, the units of which are six-membered double rings. Each screw axis contributes three molecules to such a hexamer, formed around an inversion center. The six molecules are surrounded by an inner $R_6^4(12)$ ring (Fig. 5) and an outer $R_6^6(32)$ ring. The two rings are built up from the same six hydrogen bonds in the clockwise and anticlockwise directions.

In (II) the small molecules, free from the bulky *tert*-butyl moieties, are arranged in parallel helices. The close packing of (II) is also characterized by the graphical symbols applied in Fig. 9. A full turn of the helix generates three molecules (Fig. 10), which are then joined into a four-membered ring by a molecule from the adjacent helix with opposite chirality. Thus, a novel $R_4^3(12)$ ring (Fig. 5) is formed, in which half of the hexameric $R_6^4(12)$ ring is embedded. This means that it also incorporates all three types of hydrogen bond in the crystal. The carbon-free $C_3^2(6)$ chain (formed by the N—H···O hydrogen bond) is supplemented to a full ring by a six-membered O═C(H)—C(H)—C—OH molecular fragment. The parallel (II) *versus* antiparallel (III) array of the *H* motifs can be attributed to the smaller volume of molecule (II) (by 33.5%), which gives rise to a packing coefficient (0.68) greater than that for (III) (0.63).

Finally, apart from the OH → NH_2 replacement, elimination of the *tert*-butyl moiety from (IV), (V) and (VI) equally results in the same molecule (I). Of the three packing forms assumed by (IV), (V) and (VI), the pattern hea1 found in (V) shows the highest similarity with structure (I). As indicated by the dotted lines in the graphical model (Fig. 6*b*), structure (I) forms the central part of structure (V) (Fig. 4). From the O3—H···O1 → N3—H···O1 replacement, it follows that (1a), the common tetrameric synthon (Fig. 5) of (IV) and (V), is an enlarged form of the supramolecular synthon (3) of Desiraju (1995) in structure (I). It is also a homodromic ring (Jeffrey & Saenger, 1991), labeled (3a) in Fig. 5.

3.2.4. Similarities in terms of graphs and synthons. Within the observed five forms of close packing, the 2-OH and 1-COOH (IV)–(VI) or $CONH_2$ (I)–(III) functions are the network builders *via* the same two hydrogen bonds (O1—H···O2 and *X*3—H···O1), while the *cis*/*trans* isomerism and the bulky *tert*-butyl group are the pattern modifiers. It may be concluded that the exclusive formation of the homodromic O—H···O═C—*R* motif with the $C(6)$ graph is common in the six crystal structures. The *cis* or *trans* stereoisomerism, *i.e.* the chirality of C1 and C2, excludes the formation of any intramolecular hydrogen bond, but it also governs the symmetry of the principal hydrogen bonds.

The second hydrogen bond, O═C—*X*—H···OH (*X* = O or NH), plays a complementary role in the formation of the patterns. For example, by forming homodromic $R_2^2(12)$ dimers in (III) and (IV), it connects the antiparallel *H* and *T* chains, respectively. It also takes part in the formation of the new synthons (1a) or (3a). The role of the third, N3—H3*d*···O2 hydrogen bond is less obvious. In (III) it is coupled to the principal hydrogen bond, forming together homodromic and homochiral $R_2^2(10)$ rings (Fig. 11), while in (II) it is associated with the second hydrogen bond. However, here the homodromic $R_2^2(10)$ rings are heterochiral (Fig. 12). The N3—

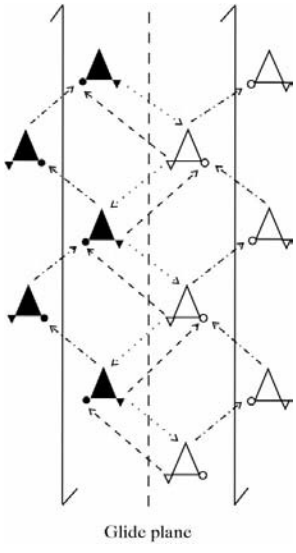

Figure 10
Pattern hop1: parallel helices define structure (II). A full turn of either helix involves three O1—H···O2 hydrogen-bonded molecules. They complete an $R_4^3(12)$ ring when an adjacent molecule from the parallel enantiomeric helix donates two NH···O hydrogen bonds. Between the parallel helices, there is a glide plane *c* which organizes these two NH···O hydrogen bonds into infinite chains running in opposite directions.

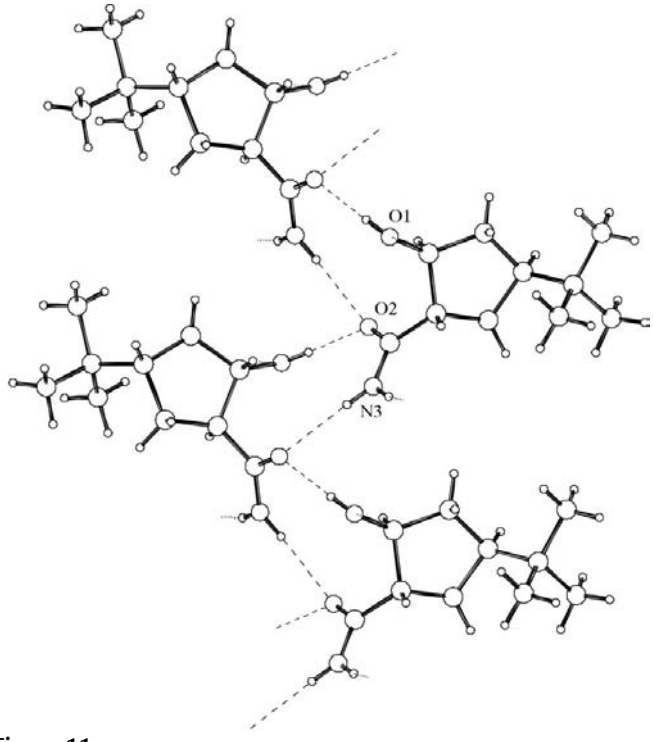

Figure 11
A fragment of structure (III) showing the screw-axis-generated helix of the adjacent $R_2^2(10)$ rings. Each pair shares a common bond, C6—O2.

H3$d\cdots$O2 hydrogen bond also assists in the formation of an $R_6^4(12)$ (III) and a heterodromic $R_4^3(12)$ ring (II). The carbon-free $R_6^4(12)$ ring of (III) is an enlarged form of synthon (3a) (Fig. 5). In this ring, both arms of the NH_2 moiety contribute to the hydrogen-bond network: the first to the dimer and the second to the helix. Accordingly, the adjoining $CONH_2$ group is forced into the outer ring. It is therefore replaced by the carbonyl O atom from a third molecule, provided by a half turn of the screw axis. Thus, the heterodromic ring (Jeffrey & Saenger, 1991) remains 12-membered with the same number of acceptors (four), while the number of donors is increased to six. In our opinion, the $R_6^4(12)$ ring in (III) inherits the structure-cementing properties of the $R_4^4(12)$ tetramers. In addition, there is a genetic connection between synthons (3) and (3a) and ring (3b).

In (I), as a real supramolecular synthon (4) (Desiraju, 1995), the N3—H3$d\cdots$O2 hydrogen bond seems to stabilize the network retained from (V). This can be attributed to the topologically different glide planes $c(x, \frac{1}{4}, z)$ and $c(x, \frac{3}{4}, z)$ in space group $P2_1/c$ (Table 3). Similarly, as in (V), the N3—H3$c\cdots$O1 hydrogen bonds form homochiral $C(6)$ chains of molecules related by the screw axes, while the $C(6)$ chains of the O1—H$\cdots$O2 hydrogen bonds are ordered along the glide plane c $(x, \frac{1}{4}, z)$. The N3—H3$d\cdots$O2 hydrogen bond, forming shorter $C(4)$ chains, preserves their glide plane symmetry, but the plane is c $(x, \frac{3}{4}, z)$. As shown in Fig. 13, four molecules related by these independent glide planes form a large antidromic $R_4^3(18)$ ring, with two O1—H$\cdots$O2 hydrogen bonds on the right side and two N3—H3$d\cdots$O2 hydrogen bonds on the left side. Thus, these parallel hydrogen-bond chains bound to the common 'bifurcated' acceptor atom O2 have a cooperative effect on the close packing of (I). By means of these forces (I) has the highest packing coefficient (0.72) among the six structures.

The graph sets discussed above are basically determined by four intramolecular chains: a seven-membered chain with two donor atoms and no acceptor atoms, denoted ${}_2 7^0$, a six- and a four-membered chain with one donor atom and one acceptor atom, denoted ${}_1 6^1$ and ${}_1 4^1$, respectively, and a five-membered chain with no donor atom, but with two acceptor atoms, denoted ${}_0 5^2$:

$$
\begin{aligned}
{}_2 7^0 &: \mathrm{H}-X-\mathrm{C(O)}-\mathrm{C}-\mathrm{C}-\mathrm{O}-\mathrm{H}\\
{}_1 6^1 &: \mathrm{O}-\mathrm{C}-\mathrm{C}-\mathrm{C}-\mathrm{O}-\mathrm{H}\\
{}_1 4^1 &: \mathrm{O}-\mathrm{C}-X-\mathrm{H}\\
{}_0 5^2 &: \mathrm{O}-\mathrm{C}-\mathrm{C}-\mathrm{C}-\mathrm{O}.
\end{aligned}
$$

In cooperation with individual OH group(s) or carbonyl O atom(s), they generate larger chains and rings. Partitioning of the large rings or chains into molecular fragments by the use of these subunit notations (Table 4) may help reveal further similarities. The arrows in the partitioned graph-set notations facilitate a distinction between the homo-, anti- and heterodromic characters of the hydrogen bonds organized in the rings discussed above. Interestingly, (I), (IV) and (V) all involve the homodromic $R_4^4(12)$ tetramer. Even among different heterodromic graph sets, formed with the third hydrogen bonds, (II) and (III) have homodromic $R_6^6(24)$ and $R_4^4(18)$ rings, respectively, which contribute to the stability of their close packing (Jeffrey & Saenger, 1991). Only in (VI), which exhibits polymorphism (Riddell *et al.*, 1995), is the principal $R_4^4(18)$ ring antidromic. It is to be hoped that when further structures become available, they can be utilized for an

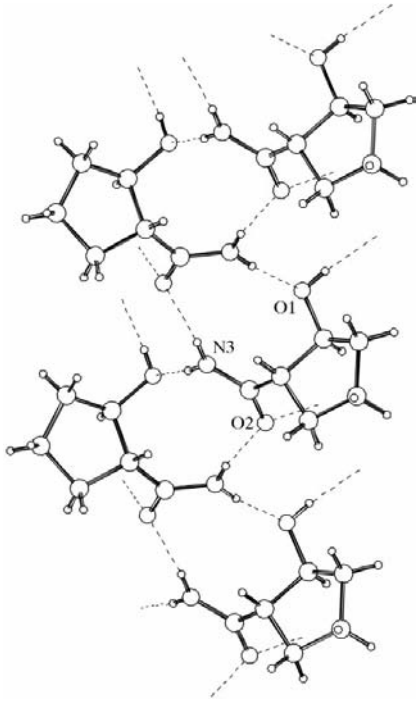

Figure 12
Parallel helices in (II), linked by an infinite row of heterochiral $R_2^2(10)$ rings. Each pair shares a common bond, C6—N3.

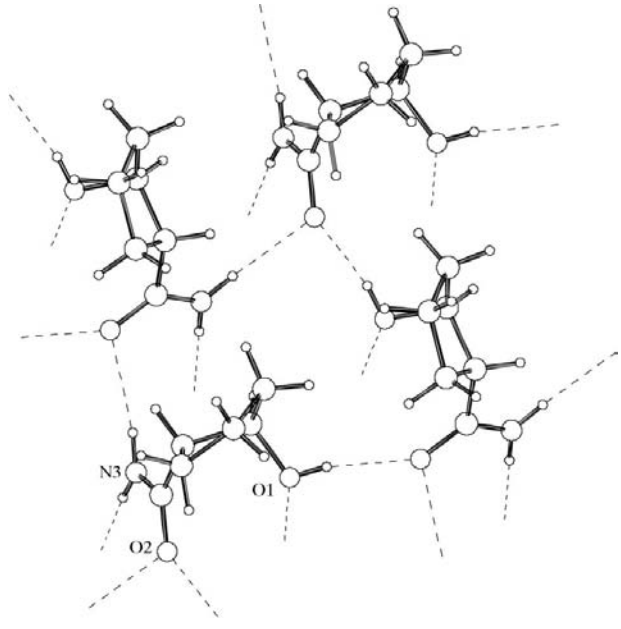

Figure 13
An antidromic $R_4^3(18)$ ring completed by O1—H$\cdots$O2 and N3—H3$d\cdots$O2 chains between four molecules of (I).

Table 4
Graph-set notations, $R_d^a(n)$ of the largest rings ($n \geq 18$) partitioned in terms of the ring components.

Arrows indicate the donor → acceptor directions, which determine the homo,-hetero- and antidromic character of the rings.

(I): $R_3^3(18)$: $\leftarrow {}_27^0 \rightarrow {}_14^1 \rightarrow {}_01^1 \leftarrow {}_16^1 \leftarrow$	Antidromic
(II): $R_4^4(18)$: $\rightarrow {}_16^1 \rightarrow {}_12^1 \rightarrow {}_16^1 \rightarrow {}_14^1 \rightarrow$	Homodromic
(III): $R_6^6(32)$: $\leftarrow {}_14^1 \leftarrow {}_27^0 \rightarrow {}_05^2 \leftarrow {}_14^1 \leftarrow {}_27^0 \rightarrow {}_05^2 \leftarrow$	Heterodromic
(III): $R_6^6(24)$: $\rightarrow {}_16^1 \rightarrow {}_14^1 \rightarrow {}_12^1 \rightarrow {}_16^1 \rightarrow {}_14^1 \rightarrow {}_12^1 \rightarrow$	Homodromic
(I), (V): $R_4^4(24)$: $\leftarrow {}_27^0 \rightarrow {}_05^2 \leftarrow {}_27^0 \rightarrow {}_05^2 \leftarrow$	Heterodromic
(VI): $R_4^4(18)$: $\leftarrow {}_27^0 \rightarrow {}_14^1 \rightarrow {}_05^2 \leftarrow {}_12^1 \leftarrow$	Antidromic

understanding of deeper connections between these supramolecular self-organizations.

3.3. Isostructurality of (I) and (V)

The similar tetrameric supramolecular synthon [(1a) or (3a)] of (V) and (I), stabilized by the cooperative effect of the $C(4)$ and $C(6)$ chains in the latter, called our attention (Kálmán *et al.*, 2000) to a novel case of isostructurality (Kálmán *et al.*, 1993) between two small molecules substantially differing both in volume (by 33.5%) and in shape. This suggests to reconsider the early view of Kitaigorodskii (1961) on the condition and limits of isomorphism. Such a relaxed form of isostructurality, in which the requirement of molecular isometricity is not fulfilled, but the packing arrangement is preserved, is termed homostructurality (Kálmán & Párkányi, 1997). Homostructurality is shown *e.g.* by the structures of Ph_4C (Robbins *et al.*, 1975) and Ph_4Pb (Busetti *et al.*, 1967) with similar shape but different volume (by ∼10–15%) and diphenyldiacyloxyspirosulfurane (Kálmán *et al.*, 1973) and its binaphthyl analog (Kapovits *et al.*, 1993) differing both in size (∼26%) and shape. Quantitatively, such pairs are characterized by a low volumetric index (*ca* 50%) of isostructurality (Fábián & Kálmán, 1999). The $R_4^4(12)$ ring, regarded as a tetrameric supramolecular synthon, is the hallmark of the observed structural similarities in (I), (IV) and (V). The vicinal (1,2-*cis*) position of a pair of donor/acceptor functions located on a small, but flexible spacer seems to account for this phenomenon. The homostructurality of (I) and (V) underscores (Fig. 14) the priority of the antiparallel and heterochiral chains using both $2_1/c$ operators in the most frequent space group $P2_1/c$ (35.5%) in the Cambridge Structural Database (CSD; Allen & Kennard, 1993). It must be emphasized that (I) and (V) are homostructural, but not isomorphous (*cf.* the lattice parameters in Table 1).

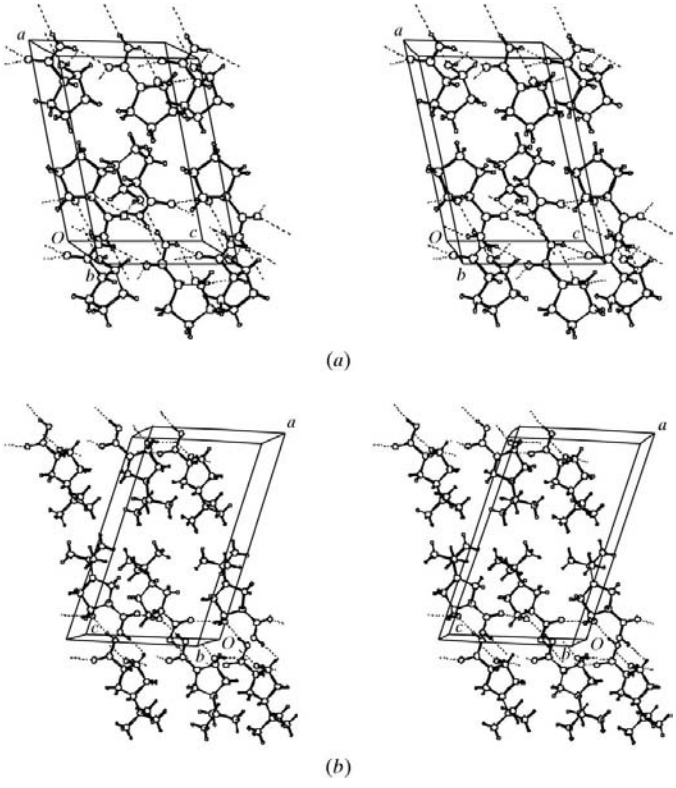

Figure 14
Stereoviews of the structural layouts of (*a*) (I) and (*b*) (V) showing projections *ac versus ca* projected onto $+b$ (I) and the $-b$ (V) axis. Structure (I) can clearly be recognized in the center of the layout of (V).

4. Conclusions

It has been demonstrated that six structures (I)–(VI) reflect five distinct forms of supramolecular self-assembly. They are formed by parallel or antiparallel hydrogen-bonded molecular chains. Since each crystal is racemic, the molecular chains are either homo- or heterochiral. Two additional patterns can be generated if the *H* (helix) motif is replaced by the *R* (ring) motif in the pattern hea1 and by the *T* (tape) motif in the pattern hop1. They are termed hea2 (Fig. 8*c*) and hop2. A third pattern (hep2) may also be expected if the *n* glide-plane-generated *M* motifs in pattern hep1 are replaced by two meanders generated by parallel glide planes, *e.g. a* and *c*.

These conclusions are valid (i) only for solvate-free crystals and (ii) if the roles of the different hydrogen bonds O—H···O=C and O—H···O—H are not interchangeable. The formation of hydrates cannot be excluded and a survey of the homodromic $R_4^4(12)$ tetramers separated by $R_2^2(12)$ dimers (Fig. 3) implies the possibility of such an exchange of functions.

To shed light on these questions, appropriately chosen novel compounds are to be synthesized and crystallized: (i) with enlarged, six-, seven- and eight-membered spacer rings, and (ii) with novel ring substituents (*e.g.* methyl, ethyl, propyl *etc.*). Since the initial submission of this paper (1*R**,2*S**)-2-hydroxy-1-cyclohexane- and -1-cycloheptanecarboxylic acids have already been subjected to X-ray crystallography.[2] Both were found to crystallize in a monoclinic system with space group $C2/c$. Thus, the $R_4^4(12)$ tetramers are retained around the twofold axes separated by $R_2^2(12)$ dimers in accordance with the predicted pattern hea2 (Fig. 6*c*). It is noteworthy that their close packings again exhibit homostructurality.

[2] Details of these structure determinations along with those of other cyclohexane, cycloheptane and cyclooctane carboxylic acids which have been synthesized will be published by the authors in this journal in due course.

Accordingly, the results presented here and the work in progress may help crystal engineering (even structure prediction, see pattern hea2) through exploration of the effects of weak van der Waals forces in the choice of the sterically and energetically most favorable (or alternative) packing forms.

The structure analyses were supported by OTKA grant No. T023212 (and partly T034985) and the synthetic work by OTKA grant No. T030647. Thanks are due to Mr Csaba Kertész and Mrs Györgyi Tóth-Csákvári for their technical assistance.

References

Allen, F. H. & Kennard, O. (1993). *Chem. Des. Autom. News*, **8**, 31–37.
Altona, C., Geise, H. J. & Romers, C. (1968). *Tetrahedron*, **24**, 13–32.
Bernáth, G., Láng, K. L., Göndös, Gy., Márai, P. & Kovács, K. (1972). *Acta Chim. Hung.* **74**, 479–497.
Bernáth, G. & Svoboda, M. (1972). *Tetrahedron*, **28**, 3475–3484.
Bernáth, G., Szakonyi, Zs., Fülöp, F. & Sohár, P. (1994). *Heterocycles*, **37**, 1687–1694.
Bernstein, J., Davis, R. E., Shimoni, L. & Chang, N.-L. (1995). *Angew. Chem. Int. Eng. Ed.* **34**, 1555–1573.
Busetti, V., Mammi, M., Signor, A. & DelPra, A. (1967). *Inorg. Chim. Acta*, **1**, 424–428.
Brock, C. P. & Dunitz, J. D. (1994). *Chem. Mater.* **6**, 1118–1127.
Cremer, D. & Pople, J. A. (1975). *J. Am. Chem. Soc.* **97**, 1354–1358.
Desiraju, G. R. (1995). *Angew. Chem. Int. Eng. Ed.* **34**, 2311–2327.
Desiraju, G. R. (1997). *Chem. Commun.* pp. 1475–1482.
Dunitz, J. D. & Bernstein, J. (1995). *Acc. Chem. Res.* **28**, 193–200.
Enraf–Nonius (1992). *CAD*-4 *Express Manual*. Enraf–Nonius, Delft, The Netherlands.
Etter, M. C. (1990). *Acc. Chem. Res.* **23**, 120–126.
Fábián, L. & Kálmán, A. (1999). *Acta Cryst.* B**55**, 1099–1108.
Flack, H. D. (1983). *Acta Cryst.* A**39**, 876–881.
Fülöp, F., Bernáth, G., Spitzner, R., Mattinen, J. & Pihlaja, K. (1994). *Acta Chim. Hung.* **131**, 435–443.
Gavezzotti, A. (1983). *J. Am. Chem. Soc.* **105**, 5220–5225.
Harms, K. (1996). *XCAD*4. Philipps-University of Marburg, Germany.
Jeffrey, G. A. & Saenger, W. (1991). *Hydrogen Bonding in Biological Structures*. Berlin, Heidelberg: Springer Verlag.
Kálmán, A., Fábián, L. & Argay, Gy. (2000). *Chem. Commun.* pp. 2255–2256.
Kálmán, A. & Párkányi, L. (1997). *Adv. Mol. Struct. Res.* **3**, 189–226.
Kálmán, A., Párkányi, L. & Argay, Gy. (1993). *Acta Cryst.* B**49**, 1039–1049.
Kálmán, A., Sasvári, K. & Kapovits, I. (1973). *Acta Cryst.* B**29**, 355–357.
Kapovits, I., Rábai, J., Szabó, D., Czakó, K., Kucsman, Á., Argay, Gy., Fülöp, V., Kálmán, A., Koritsánszky, T. & Párkányi, L. (1993). *J. Chem. Soc. Perkin Trans. 2*, pp. 847–853.
Kitaigorodskii, A. I. (1961). *Organic Chemical Crystallography*, pp. 222–231. New York: Consultants Bureau.
Riddell, F. G., Bernáth, G. & Fülöp, F. (1995). *J. Am. Chem. Soc.* **117**, 2327–2335.
Robbins, A., Jeffrey, G. A., Chesick, J. P., Donohue, J., Cotton, F. A., Frenz, B. A. & Murillo, C. A. (1975). *Acta Cryst.* B**31**, 2395–2399.
Spek, A. L. (1998). *PLATON*. University of Utrecht, The Netherlands.
Sheldrick, G. M. (1985) *SHELXS*86. University of Göttingen, Germany.
Sheldrick, G. M. (1997*a*). *SHELXS*97. University of Göttingen, Germany.
Sheldrick, G. M. (1997*b*). *SHELXL*97. University of Göttingen, Germany.
Szakonyi, Zs., Fülöp, F., Bernáth, G. & Sohár, P. (1996). *Heterocycles*, **42**, 625–634.
Zorky, P. M. (1993). *Acta Chim. Hung.* **130**, 173–181.